A Preconditioned Inexact Newton Method for Nonlinear Sparse Electromagnetic Imaging

Abdulla Desmal, *Student Member, IEEE*, and Hakan Bağcı, *Member, IEEE*

***Abstract*—A nonlinear inversion scheme for the electromagnetic microwave imaging of domains with sparse content is proposed. Scattering equations are constructed using a contrast–source (CS) formulation. The proposed method uses an inexact Newton (IN) scheme to tackle the nonlinearity of these equations. At every IN iteration, a system of equations, which involves the Frechet derivative (FD) matrix of the CS operator, is solved for the IN step. A sparsity constraint is enforced on the solution via thresholded Landweber iterations, and the convergence is significantly increased using a preconditioner that levels the FD matrix's singular values associated with contrast and equivalent currents. To increase the accuracy, the weight of the regularization's penalty term is reduced during the IN iterations consistently with the scheme's quadratic convergence. At the end of each IN iteration, an additional thresholding, which removes small "ripples" that are produced by the IN step, is applied to maintain the solution's sparsity. Numerical results demonstrate the applicability of the proposed method in recovering sparse and discontinuous dielectric profiles with high contrast values.**

***Index Terms*—Electromagnetic (EM) imaging, inexact Newton (IN), sparse optimization, thresholded Landweber (LW).**

I. Introduction

THE formulation and implementation of methods for solving inverse electromagnetic (EM) scattering problems have been an active research topic in the last three decades due to their applications in various fields including nondestructive evaluation, radar and remote sensing, crack detection, through-wall imaging, and hydrocarbon reservoir exploration. In almost all of these applications, the nonlinearity and ill posedness of the inverse EM scattering problem must be tackled [1].

Inversion methods can be classified depending on how they tackle the nonlinearity. When scattered fields are weak, first-order Born and Rytov methods [2] can be used accurately. However, as the contrast in the investigation domain increases, more rigorous methods have to be used. The accuracy of the reconstruction increases as one moves from extended and second-order Born approximations and the iterative Born method [3] to "fully" nonlinear distorted Born [4], Levenberg–Marquardt [5], and inexact Newton (IN) [6] schemes.

Manuscript received April 11, 2014; revised August 6, 2014; accepted August 14, 2014. Date of publication September 4, 2014; date of current version September 16, 2014.

A. Desmal is with the Division of Computer, Electrical, and Mathematical Sciences and Engineering, King Abdullah University of Science and Technology, Thuwal 23955-6900, Saudi Arabia (e-mail: abdulla.desmal@kaust.edu.sa).

H. Bağcı is with the Division of Computer, Electrical, and Mathematical Sciences and Engineering and the Center for Uncertainty Quantification in Computational Science and Engineering, King Abdullah University of Science and Technology, Thuwal 23955-6900, Saudi Arabia (e-mail: hakan.bagci@kaust.edu.sa).

Color versions of one or more of the figures in this paper are available online at http://ieeexplore.ieee.org.

Digital Object Identifier 10.1109/LGRS.2014.2349935

The ill posedness of the inverse problem is circumvented via regularization schemes, which minimize a cost function weighted between a penalty term and the L_2-norm of the mismatch between the model's scattered fields and measurements. The most common scheme, i.e., the Tikhonov regularization, uses the L_2-norm of the solution as the penalty term. It is well known that this promotes smoothness in the solution. Recently, sparsity-promoting regularization schemes, which use the L_0/L_1-norm penalty terms, have gained popularity in signal processing communities for linear image recovery due to their efficiency and accuracy in recovering sparse and discontinuous solutions [7], [8]. Their use in inverse EM scattering problems have been only limited to linearized inversion methods [9], which are only applicable on investigation domains populated with low-contrast scatterers.

To this end, in this letter, a nonlinear inversion method for the EM imaging of sparse domains is proposed. The scattering equations are constructed using a contrast–source (CS) formulation [10] since it allows both contrast and (equivalent) source samples to be sparse at the same time (as opposed to a contrast–field formulation where field samples are not immediately sparse). The nonlinearity is tackled using the IN algorithm [6]. At every IN iteration, the proposed INCS calls for the solution of a system of equations, which involves the Frechet derivative (FD) matrix of the discretized CS operator, for the IN step. The sparsity regularization is enforced on this solution via thresholded Landweber (LW) iterations. However, a naive application of this scheme results in slow convergence since the FD matrix's singular values that are associated with CS components typically vary by a few orders of magnitude. To this end, a preconditioning procedure is applied to the FD matrix during LW iterations. This avoids the "loss of information" by leveling the singular values associated with the FD matrix's CS components. Preconditioning significantly increases the convergence rate. Additionally, to increase the accuracy, the weight of the regularization's penalty term is reduced during the IN iterations consistently with the scheme's quadratic convergence. At the end of each IN, an additional thresholding, which removes small "ripples" that are produced by the modifications in the IN step, is applied. This helps maintain the solution's sparsity and significantly increases the effectiveness of the regularization.

The numerical results presented in this letter demonstrate the superiority of the proposed sparsity-regularized INCS method in recovering sparse and discontinuous dielectric profiles with high contrast values.

II. Formulation

A. CS Formulation

Let S^d represent the support of the investigation domain residing in the unbounded 2-D space. Let $\varepsilon(\mathbf{r})$ represent the

permittivity. Inside the investigation domain ($\mathbf{r} \in S^d$), $\varepsilon(\mathbf{r})$ is unknown, and in the background medium, $\varepsilon(\mathbf{r}) = \varepsilon_0$. The permeability of both the investigation domain and the background medium is μ_0. S^d is surrounded by N^t line sources. Let $E_i^i(\mathbf{r})$ represent the incident electric field generated by the ith source. Upon illumination by $E_i^i(\mathbf{r})$, the equivalent electric current density $J_i(\mathbf{r})$ is induced on S^d, and $J_i(\mathbf{r})$ generates scattered field $E_i^s(\mathbf{r})$. Let $E_i(\mathbf{r})$ represent the total electric field. Enforcing $E_i(\mathbf{r}) = E_i^i(\mathbf{r}) + E_i^s(\mathbf{r})$ for $\mathbf{r} \in S^d$ and noting that $J_i(\mathbf{r}) = \tau(\mathbf{r})E_i(\mathbf{r})$, where $\tau(\mathbf{r}) = \varepsilon(\mathbf{r})/\varepsilon_0 - 1$ is the contrast, yield [10]

$$L_i^d(\tau,\, J_i) = J_i(\mathbf{r}) - \tau(\mathbf{r})E_i^i(\mathbf{r}) - k_0^2\tau(\mathbf{r}) \int_{S^d} J_i(\mathbf{r}')G(\mathbf{r},\, \mathbf{r}')\, ds' = 0, \quad \mathbf{r} \in S^d. \tag{1}$$

Here, $G(\mathbf{r},\, \mathbf{r}') = H_0^{(2)}(k_0|\mathbf{r} - \mathbf{r}'|)/(4j)$ is the 2-D Green function, $k_0 = \omega\sqrt{\varepsilon_0\mu_0} = 2\pi/\lambda_0$ is the wavenumber, ω is the frequency, λ_0 is the wavelength, and $H_0^{(2)}(\cdot)$ is the second kind Hankel function. Let S^r represent the observation domain, where $E_i^s(\mathbf{r})$ are given by

$$E_i^s(\mathbf{r}) = L_i^r(J_i) = k_0^2 \int_{S^d} J_i(\mathbf{r}')G(\mathbf{r},\, \mathbf{r}')\, ds', \quad \mathbf{r} \in S^r. \tag{2}$$

Equations (1) and (2) represent the well-known CS formulation [10]. Assume that $E_i^s(\mathbf{r})$ measured at $\mathbf{r} \in S^r$ are known and denoted by $E_i^r(\mathbf{r})$. Then, $\tau(\mathbf{r})$ can be obtained from $E_i^r(\mathbf{r})$ by solving

$$L(z) - y = 0 \tag{3}$$

which is constructed by cascading (1) and (2) for all sources. Here, $z(\mathbf{r}) = [\tau(\mathbf{r}), J_1(\mathbf{r}), \ldots, J_{N^t}(\mathbf{r})]^t$, $y(\mathbf{r}) = [0, \ldots, 0, E_1^r(\mathbf{r}), \ldots, E_{N^t}^r(\mathbf{r})]^t$, and $L(z) = [L_1^d(\tau, J_1), \ldots, L_{N^t}^d(\tau, J_{N^t}), L_1^r(J_1), \ldots, L_{N^t}^r(J_{N^t})]^t$.

B. IN Formulation

Equation (3) describes a nonlinear relation in unknown variable $z(\mathbf{r})$. This suggests that it can be solved using a Newton-type method with quadratic convergence [6]. Indeed, the IN method has been used together with the CS formulation in solving the EM inverse scattering problem [6]. The IN iteratively finds the zeros of (3). The iteration k of this algorithm reads

$$F\left[L(z)\right]|_{z_k}\left(\Delta z_{(k)}\right) = y - L\left(z_{(k)}\right), \qquad z_{(k+1)} = z_{(k)} + \Delta z_{(k)}. \tag{4}$$

Here, subscript (k) indicates that the variables it is attached to belong to IN iteration k, operator $F[L(z)]|_{z_{(k)}}(\Delta z_{(k)})$ returns the first-order multivariate FD of $L(z)$ evaluated at $z = z_{(k)}$ and applied to $\Delta z_{(k)}$, and $\Delta z_{(k)} = [\Delta\tau_{(k)},\, \Delta J_{1(k)}, \ldots, \Delta J_{N^t(k)}]^t$ is the IN step at iteration k. Let operators $\partial_{J_i}[L_i^d(\tau,\, J_i)](\Delta J_i)$, $\partial_\tau[L_i^d(\tau,\, J_i)](\Delta\tau)$, and $\partial_\tau[L_i^r(\tau)](\Delta\tau)$ represent the functional derivatives of $L_i^d(\tau,\, J_i)$ and $L_i^r(\tau)$ with respect to J_i and τ, respectively, and operate on ΔJ_i and $\Delta\tau$, respectively. From (1) and (2), one can obtain the expressions of these operators as

$$\partial_{J_i}\left[L_i^d(\tau,\, J_i)\right](\Delta J_i) = \Delta J_i(\mathbf{r}) - k_0^2\tau(\mathbf{r}) \int_{S^d} G(\mathbf{r},\, \mathbf{r}')\Delta J_i(\mathbf{r}')\, ds', \quad \mathbf{r} \in S^d$$

$$\partial_\tau\left[L_i^d(\tau,\, J_i)\right](\Delta\tau) = \Delta\tau(\mathbf{r})\left[-E_i^i(\mathbf{r}) - k_0^2 \int_{S^d} J_i(\mathbf{r}')G(\mathbf{r},\, \mathbf{r}')\, ds'\right], \quad \mathbf{r} \in S^d$$

$$\partial_{J_i}\left[L_i^r(J_i)\right](\Delta J_i) = k_0^2 \int_{S^d} G(\mathbf{r},\, \mathbf{r}')\Delta J_i(\mathbf{r}')\, ds', \quad \mathbf{r} \in S^r. \tag{5}$$

Additionally, $L_i^d(\tau,\, J_i)$ only depends on $\tau(\mathbf{r})$ and $J_i(\mathbf{r})$, and $L_i^r(J_i)$ only depends on $J_i(\mathbf{r})$. Therefore, $\partial_{J_m}[L_i^d(\tau,\, J_i)](\cdot) = 0$ and $\partial_{J_m}[L_i^r(J_i)](\cdot) = 0$ for $i \neq m$, and $\partial_\tau[L_i^r(J_i)](\cdot) = 0$ for $i = 1, \ldots, N^t$. Consequently, $F[L(z)]|_{z_{(k)}}$ is expressed in the form of a sparse matrix with nonzero entries as follows:

$$\left\{F\left[L(z)\right]|_{z_{(k)}}\right\}_{i,\,1} = \partial_\tau\left[L_i^d(\tau,\, J_i)\right]\big|_{z_{(k)}}$$

$$\left\{F\left[L(z)\right]|_{z_{(k)}}\right\}_{i,\,i+1} = \partial_{J_i}\left[L_i^d(\tau,\, J_i)\right]\big|_{z_{(k)}}$$

$$\left\{F\left[L(z)\right]|_{z_{(k)}}\right\}_{i+N^t,\,i+1} = \partial_{J_i}\left[L_i^r(J_i)\right]|_{z_{(k)}}.$$

C. Discretization

To discretize (4), S^d is divided into N^d square cells, and S^r is probed with N^r measurements. The centers of the square cells and the locations of the measurement samples are denoted by $\mathbf{r}_n^d$, $n = 1, \ldots, N^d$, and $\mathbf{r}_m^r$, $m = 1, \ldots, N^r$, respectively. Quantities defined on S^d are approximated as

$$\tau(\mathbf{r}) \approx \sum_{n=1}^{N^d}\{\bar{\tau}\}_n p_n(\mathbf{r}),\; J_i(\mathbf{r}) \approx \sum_{n=1}^{N^d}\{\bar{J}_i\}_n p_n(\mathbf{r})$$

$$\Delta\tau(\mathbf{r}) \approx \sum_{n=1}^{N^d}\{\Delta\bar{\tau}\}_n p_n(\mathbf{r}),\; \Delta J_i(\mathbf{r}) \approx \sum_{n=1}^{N^d}\{\Delta\bar{J}_i\}_n p_n(\mathbf{r}) \tag{6}$$

where $\{\bar{\tau}\}_n = \tau(\mathbf{r}_n^d)$, $\{\bar{J}_i\}_n = J_i(\mathbf{r}_n^d)$, $\{\Delta\bar{\tau}\}_n = \Delta\tau(\mathbf{r}_n^d)$, $\{\Delta\bar{J}_i\}_n = \Delta J_i(\mathbf{r}_n^d)$, and $p_n(\mathbf{r})$ is the pulse basis function on cell n with support S_n and is nonzero only for $\mathbf{r} \in S_n$ with unit amplitude. Inserting (6) into (4) and evaluating the resulting equation at $\mathbf{r}_p^d$, $p = 1, \ldots, N^d$, and $\mathbf{r}_m^r$, $m = 1, \ldots, N^r$, yield

$$\bar{F}_{(k)}\Delta\bar{z}_{(k)} = \bar{y} - \bar{L}\left(\bar{z}_{(k)}\right) \tag{7}$$

where $\bar{z}_{(k)} = [\bar{\tau}_{(k)}^t,\, \bar{J}_{1(k)}^t, \ldots, \bar{J}_{N^t(k)}^t]^t$, $\Delta\bar{z}_{(k)} = [\Delta\bar{\tau}_{(k)}^t,\, \Delta\bar{J}_{1(k)}^t, \ldots, \Delta\bar{J}_{N^t(k)}^t]^t$, $\bar{y} = [\bar{0}^t, \ldots, \bar{0}^t,\, \bar{E}_1^{r,\,t}, \ldots, \bar{E}_{N^t}^{r,\,t}]^t$ with $\{\bar{E}_i^r\}_m = E_i^r(\mathbf{r}_m^r)$, and the nonzero entries of $\bar{L}(\bar{z}_{(k)})$ and $\bar{F}_{(k)}$ are

$$\left\{\bar{L}\left(\bar{z}_{(k)}\right)\right\}_{(i-1)N^d+p} = \left\{\bar{J}_{i(k)} - D\left[\bar{\tau}_{(k)}\right]\bar{E}_i^i - D\left[\bar{\tau}_{(k)}\right]\bar{G}^d\bar{J}_{i(k)}\right\}_p$$

$$\left\{\bar{L}\left(\bar{z}_{(k)}\right)\right\}_{N^tN^d+(i-1)N^r+m} = \left\{\bar{G}^r\bar{J}_{i(k)}\right\}_m$$

$$\left\{\bar{F}_{(k)}\right\}_{(i-1)N^d+n,\,n} = \left\{D\left[-\bar{E}_i^i - \bar{G}^d\bar{J}_{i(k)}\right]\right\}_{n,\,n}$$

$$\left\{\bar{F}_{(k)}\right\}_{(i-1)N^d+p,\,iN^d+n} = \left\{\bar{I} - D\left[\bar{\tau}_{(k)}\right]\bar{G}^d\right\}_{p,\,n}$$

$$\left\{\bar{F}_{(k)}\right\}_{N^tN^d+(i-1)N^r+m,\,iN^d+n} = \{\bar{G}^r\}_{m,\,n}.$$

Here, $\{\bar{G}^d\}_{p,n} = k_0^2\int_{S_n} G(\mathbf{r}_p^d, \mathbf{r}')ds'$, $\{\bar{G}^r\}_{m,n} = k_0^2\int_{S_n} G(\mathbf{r}_m^r, \mathbf{r}')ds'$, $\{\bar{E}_i^i\}_p = E^i(\mathbf{r}_p^d)$, and operator $D[.]$ generates a diagonal matrix with entries equal to the entries of the vector at its argument.

D. IN Iterations With Sparsity Constraint Regularization

Matrix system (7) is ill posed, and a meaningful solution can be only obtained using a regularization scheme [1]. If $\Delta\bar{z}_{(k)}$ (or $\bar{z}_{(k)}$) is sparse (i.e., many entries of $\Delta\bar{z}_{(k)}$ are zeros), the regularization can be achieved through the solution of the following optimization problem:

$$\Delta\bar{z}_{(k)} = \arg\min_{\bar{x}}\left\{0.5\left\|\bar{y}-\bar{L}(\bar{z}_k)-\bar{F}_{(k)}\bar{x}\right\|_2^2+\gamma_{(k)}\|\bar{x}\|_l\right\}. \quad (8)$$

Here, $l \in \{0, 1\}$ is the norm of the penalty term, and $\gamma_{(k)}$ is its weight. For $l = 0$, the norm operation counts the number of nonzero elements in vector $\bar{x}$, providing information about its sparseness. However, the L_0-norm penalty term makes minimization problem (8) nonconvex [7]. Consequently, it may contain more than a single infimum as a solution. This issue can be overcome by replacing the L_0-norm ($l = 0$) with the L_1-norm ($l = 1$). The resulting minimization problem is the best convex approximation to the L_0-norm nonconvex minimization problem [7]. In this letter, minimization problem (8) is solved using truncated and thresholded LW iterations [7]. Consequently, the following sparsity-regularized INCS algorithm is proposed:

0) initialize $\bar{z}_{(1)} = 0$, γ_1, δ
for $k = 1, \ldots, N_{\text{it}}^{\text{IN}}$
  1) $\Delta\bar{z}_{(k)}^{(1)} = 0$
  for $j = 1, \ldots, N_{\text{it}}^{\text{reg}}$
  2) $\Delta\bar{z}_{(k)}^{(j+1)} = T_l^{\gamma_{(k)}}(\Delta\bar{z}_{(k)}^{(j)} + \beta_{(k)}\bar{F}_{(k)}^{*}[\bar{y} - \bar{L}(\bar{z}_{(k)}) - \bar{F}_{(k)}\Delta\bar{z}_{(k)}^{(j)}])$
  end
  3) $\{\bar{z}_{(k+1)}\}_{iN^d+1:(i+1)N^d} = T_0^{A_{i(k)}}(\{\bar{z}_{(k)}+\Delta\bar{z}_{(k)}^{(j+1)}\}_{iN^d+1:(i+1)N^d}), \quad i=0,\ldots,N^t$
  4) $\gamma_{(k+1)} = \delta\gamma_{(k)}$
end

Several comments about the aforementioned algorithm are in order. First, superscript (j) indicates that the variables it is attached to belong to LW iteration j. Second, LW step $\beta_{(k)}$ should satisfy $0 < \beta_{(k)} < 2/\sigma_{1(k)}^2$ for convergence. Here, $\sigma_{1(k)}$ is the largest singular value of $\bar{F}_{(k)}$. It is very accurately approximated using a few power iterations applied to $\bar{F}_{(k)}$. Third, the LW iterations are "truncated" at $j = N_{\text{it}}^{\text{reg}}$. Fourth, for $l = 0$, the thresholding function used at Step 2, i.e., $T_0^{\gamma_{(k)}}(\cdot)$, is called a hard-thresholding function, and in the complex domain, it is defined as [8]

$$\left\{T_0^{\gamma_{(k)}}(\bar{x})\right\}_v = \{\bar{x}\}_v \frac{\max\left[|\{\bar{x}\}_v| - \gamma_{(k)}, 0\right]}{\max\left[|\{\bar{x}\}_v| - \gamma_{(k)}, 0\right] + \gamma_{(k)}}. \quad (9)$$

For $l = 1$, $T_1^{\gamma_{(k)}}(\cdot)$ is termed soft-thresholding functions, and in the complex domain, it is defined as [8]

$$\left\{T_1^{\gamma_{(k)}}(\bar{x})\right\}_v = \begin{cases} \{\bar{x}\}_v, & \text{if } |\{\bar{x}\}_v| > \sqrt{2\gamma_{(k)}} \\ 0, & \text{otherwise.} \end{cases} \quad (10)$$

Fifth, at Step 4, thresholding level $\gamma_{(k)}$ is reduced by multiplying it with parameter δ, $0 < \delta < 1$. This operation helps increase the accuracy of the solution by decreasing the weight of the penalty term in (8) as IN iterations proceed. This is fully consistent with the fact that IN step $\Delta\bar{z}_{(k)}$ quadratically shrinks to zero. The initial value of thresholding level $\gamma_{(1)}$ is determined based on the noise level in the measured scattered field samples, i.e., $\bar{E}_i^r$. Sixth, Step 3 introduces an extra thresholding to remove the small ripples (with respect to the background) generated by the modifications in IN step $\Delta\bar{z}_{(k)}$. Hard-thresholding function $T_0^{A_{i(k)}}(\cdot)$ is used at this step since it clears all the ripples beneath thresholding level $A_{i(k)}$. Here, $A_{i(k)}$ are the means of input vectors $\{\bar{z}_{(k)} + \Delta\bar{z}_{(k)}^{(j+1)}\}_{iN^d+1:(i+1)N^d}$, $i = 0, \ldots, N^t$. It should be clear from this description that $\bar{\tau}_{(k)} + \Delta\bar{\tau}_{(k)}^{(j+1)}$ and $\bar{J}_{i(k)} + \Delta\bar{J}_{i(k)}^{(j+1)}$, $i = 1, \ldots, N^t$, are thresholded at different levels, depending on their averages. Finally, the aforementioned algorithm can be used when $l = 2$ (the L_2-norm penalty term in (8), i.e., the smooth regularization) after replacing the thresholding at Step 2 with the identity operator and removing Step 3.

E. Preconditioning

The naive application of the aforementioned algorithm results in very slow convergence. This is due to the fact that $\bar{z}_{(k)}$ and $\Delta\bar{z}_{(k)}$ contain samples of the contrast and the equivalent current sources, which have values that are orders of magnitude different from each other. The effect of this scaling mismatch is also observed in $\bar{F}$ and its Hermitian conjugate $\bar{F}^*$. This can be seen from the matrix entries of $\bar{F}$, where the trace of $D\{-\bar{E}_i^i - \bar{G}^d\bar{J}_i\}$ is much higher than that of $\bar{I} - D\{\bar{\tau}\}\bar{G}^d$. Due to this mismatch, the first N^d singular values of $\bar{F}$ are much higher than its remaining N^tN^d singular values. Because of this, the LW iterations at Step 3 of the IN algorithm converge very slowly. This can be explained by using singular value decomposition (SVD) filtering factors, as it is done with Tikhonov inversion schemes [11]. Let $f_v^{(i)}$ represent the vth SVD filtering coefficient at LW iteration i, i.e., $f_v^{(i)} = 1 - (1 - \beta\sigma_v^2)^i$, where σ_v is the vth singular value of $\bar{F}$, and β is the LW step, which satisfies $0 < \beta < 2/\sigma_1^2$, where σ_1 is the largest singular value. $f_v^{(i)}$ is a measure of how much the component associated with the vth singular value contributes to the solution at iteration i. $f_v^{(i)} \approx 1$ means that the solution component associated with the vth singular value is recovered. Now, assume that $\sigma_v \approx \sigma_1$, $v = 1, \ldots, N^d$, and $\sigma_v \ll \sigma_1, v = N^d + 1, \ldots, N^d(N^t + 1)$, as required by the CS formulation. Consequently, condition $f_v^{(i)} \approx 1$ will be obtained for small values of i for $v = 1, \ldots, N^d$. However, it will take much more iterations for the same condition to be satisfied for $v = N^d + 1, \ldots, N^d(N^t + 1)$. This discussion shows that leveling the singular values of $\bar{F}$ should decrease the number of LW iterations.

In this letter, a preconditioning scheme is proposed to alleviate the effect of the scaling mismatch and increase the convergence rate of the LW iterations. First, right diagonal preconditioner $\bar{M}$ is computed using $\{\bar{M}\}_{v,v} = 1/\sqrt{\{\bar{F}^*\bar{F}\}_{v,v}}$. Then, left diagonal preconditioner $\bar{P}$ is computed using preconditioned matrix $\bar{F}\bar{M}$ and its Hermitian conjugate $\bar{M}\bar{F}^*$: $\{\bar{P}\}_{v,v} = 1/\sqrt{\{\bar{F}\bar{M}\bar{M}\bar{F}^*\}_{v,v}}$. Finally, $\bar{M}$ and $\bar{P}$ are used to precondition $\bar{F}$ and $\bar{F}^*$ as $F^S = \bar{P}\bar{F}\bar{M}$ and $F^{S*} = \bar{M}\bar{F}^*\bar{P}$, respectively.

Then, Steps 2 and 3 of the INCS algorithm are updated as

$$2)\ \Delta\bar{z}_{(k)}^{(j+1)} = T_l^{\gamma_{(k)}}\left(\Delta\bar{z}_{(k)}^{(j)} + \beta_{(k)}\bar{F}_{(k)}^{S*}\left[\bar{P}\bar{y} - \bar{P}\bar{L}\left(\bar{z}_{(k)}\right) - \bar{F}_{(k)}^{S}\Delta\bar{z}_{(k)}^{(j)}\right]\right)$$

$$3)\ \left\{\bar{z}_{(k+1)}\right\}_{iN^d+1:(i+1)N^d} = T_0^{A_{i(k)}}\left(\left\{\bar{z}_{(k)} + \bar{M}\Delta\bar{z}_{(k)}^{(j+1)}\right\}_{iN^d+1:(i+1)N^d}\right)$$

respectively. Note that $\beta_{(k)}$ should now satisfy $0 < \beta_{(k)} < 2/\sigma_{1(k)}^2$, where $\sigma_{1(k)}$ is the largest singular value of $\bar{F}_{(k)}^S$, and $A_{i(k)}$ are the means of input vectors $\{\bar{z}_{(k)} + \bar{M}\Delta\bar{z}_{(k)}^{(j+1)}\}_{iN^d+1:(i+1)N^d}$, $i = 0, \ldots, N^t$.

It should be also added here that the LW iterations can be accelerated using recently developed iterative shrinkage thresholding algorithms [8]. In this letter, a two-step iterative shrinkage thresholding algorithm is used since it increases the convergence rate of the LW iterations with no additional computational cost.

III. Numerical Results

In this section, the accuracy and efficiency of the proposed method are demonstrated via examples where field samples $\bar{E}_i^r$ are obtained from actual experiments or synthetically generated, as described next. Let $\tau^{\text{ref}}(\mathbf{r})$ and $J_i^{\text{ref}}(\mathbf{r})$, and $\{\bar{\tau}^{\text{ref}}\}_n = \tau^{\text{ref}}(\mathbf{r}_n^d)$ and $\{\bar{J}_i^{\text{ref}}\}_n = J_i^{\text{ref}}(\mathbf{r}_n^d)$ represent the actual (known) contrast and (unknown) equivalent currents in the investigation domain and their samples. Matrix system $(I - D[\bar{\tau}^{\text{ref}}]\bar{G}^d)\bar{J}_i^{\text{ref}} = D[\bar{\tau}^{\text{ref}}]\bar{E}_i^i$ is solved for J_i^{ref}. Then, actual scattered field samples, i.e., $\{\bar{E}_i^{\text{ref}}\}_m = E_i^{\text{ref}}(\mathbf{r}_m^r)$, are obtained by computing $\bar{E}_i^{\text{ref}} = \bar{G}^r\bar{J}_i^{\text{ref}}$. Finally, $\bar{E}_i^r$ are generated by adding white Gaussian noise to $\bar{E}_i^{\text{ref}}$. The level of this noise is measured in decibels using $20\log_{10}$ (SNR), where SNR represents the SNR.

In all examples, the results are obtained by the INCS method regularized with: 1) thresholded, truncated, and preconditioned LW iterations with $l = 1$ (termed as sparse-INCS and abbreviated as "SP-INCS"); and 2) truncated and preconditioned LW iterations with $l = 2$ (termed as smooth-INCS and abbreviated as "SM-INCS", see the sixth comment in Section II-D).

The relative norm errors in the contrast and the scattered field samples recovered at INCS iteration k are computed using $\text{err}_{(k)}^d = \|\bar{\tau}_{(k)} - \bar{\tau}^{\text{ref}}\|_2/\|\bar{\tau}^{\text{ref}}\|_2$ and $\text{err}_{(k)}^r = \|\bar{E}_{(k)}^s - \bar{E}^r\|_2/\|\bar{E}^r\|_2$. Here, $\bar{E}^r = [\bar{E}_1^{r,t}, \ldots, E_{N^t}^{r,t}]^t$, and $\bar{E}_{(k)}^s = [\bar{E}_{1(k)}^{s,t}, \ldots, E_{(k)N^t}^{s,t}]^t$, with $E_{i(k)}^s = \bar{G}^r\bar{J}_{i(k)}$.

A. Two Dielectric Pulses

The investigation domain of size $1.3343\lambda_0 \times 1.3343\lambda_0$ contains two cylindrical pulses with a radius of $0.1\lambda_0$ and a dielectric permittivity of 3. The distance between the centers of the pulses is represented with d_s. The transmitter–receiver configuration is described in [12]. The investigation domain is discretized using $N^d = 3025$ square cells. The sparseness level (i.e., the ratio of the number of zero samples to N) in $\bar{\tau}^{\text{ref}}$ is 3.7%.

In the first set of experiments, $d_s = 0.6\lambda_0$ and $\bar{E}_i^r$ are generated from actual measurements provided in file "twodielTM_8f" [12]. $N_{\text{it}}^{\text{reg}} = 40$ for both the SP-INCS and the SM-INCS, and $\gamma_{(1)} = 0.1$ and $\delta = 0.85$ for the SP-INCS. The solutions recovered at the SM-INCS and SP-INCS iteration $k = 35$ in are shown in Fig. 1(a) and (b), respectively. This figure shows that the image recovered by the SP-INCS is sharper and more accurate.

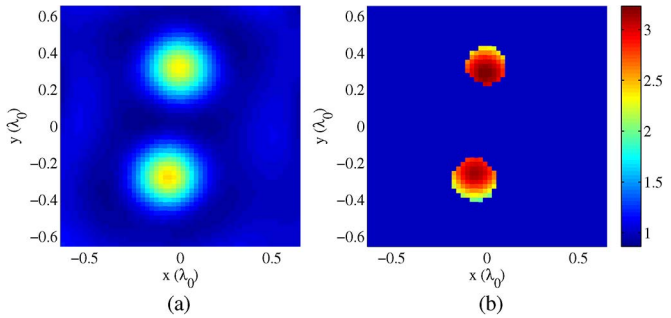

Fig. 1. Profiles recovered by the (a) SM-INCS and the (b) SP-INCS at $k = 35$.

TABLE I
$\text{err}_{(35)}^d$ Computed for Various Values of d_s

d_s	SM-INCS	SP-INCS
$0.6\lambda_0$	72%	35%
$0.4\lambda_0$	74%	43%
$0.35\lambda_0$	77%	51%
$0.3\lambda_0$	77%	58%

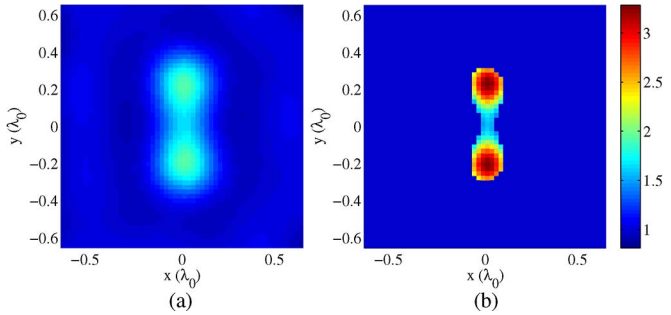

Fig. 2. Profiles recovered by the (a) SM-INCS ($\text{err}_{(35)}^d = 74\%$) and the (b) SP-INCS ($\text{err}_{(35)}^d = 43\%$) at $k = 35$.

In the second set of experiments, the conductivity of the pulses increased to 0.1 S/m, and $\bar{E}_i^r$ are synthetically generated with 20 dB noise, whereas d_s is varied between $0.3\lambda_0$ and $0.6\lambda_0$. All other parameters are kept the same. Table I lists $\text{err}_{(35)}^d$ computed by the SP-INCS and the SM-INCS. The error stays reasonably low, although the pulses are only separated by $d_s = 0.3\lambda_0$. For $d_s = 0.4\lambda_0$, the solutions recovered at the SM-INCS and SP-INCS iteration $k = 35$ in are shown in Fig. 2(a) and (b), respectively. The SP-INCS works as expected, even when the investigation domain involves lossy scatterers.

In the last set of experiments, $d_s = 0.6\lambda_0$, and the noise level in $\bar{E}_i^r$ is varied between 20 and 5 dB. All other parameters are kept the same as those in the second set of simulations. The SP-INCS produced $\text{err}_{(35)}^d = 35\%$, $\text{err}_{(35)}^d = 36\%$, $\text{err}_{(35)}^d = 42\%$, and $\text{err}_{(35)}^d = 49\%$ for noise levels of 20, 15, 10, and 5 dB, respectively.

B. Circular Ring

The relative permittivity profile of the domain and the receiver–transmitter configuration are shown in Fig. 3. The

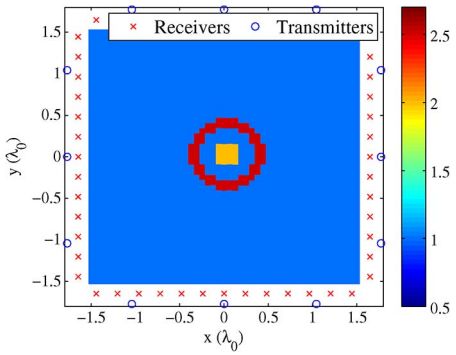

Fig. 3. Actual permittivity profile and transmitter–receiver locations.

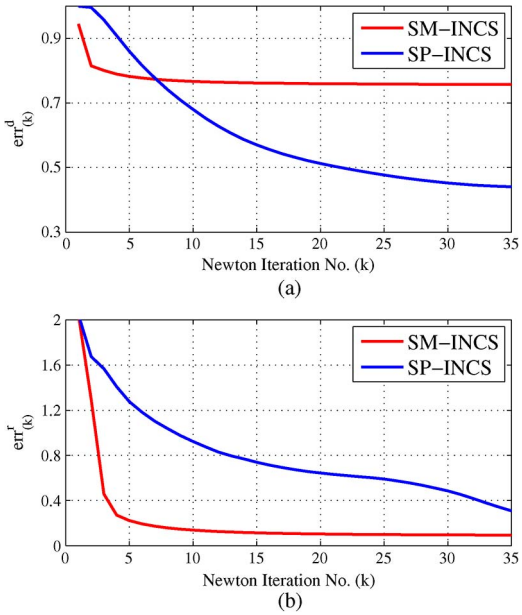

Fig. 4. (a) $\text{err}^d_{(k)}$ and (b) $\text{err}^r_{(k)}$ computed by the SM-INCS and the SP-INCS.

investigation domain is discretized using $N^d = 2500$ square cells. The sparseness level in $\bar{\tau}^{\text{ref}}$ is 3.36%. The numbers of transmitters and receivers are $N^t = 12$ and $N^r = 52$, respectively. $N_{\text{it}}^{\text{reg}} = 60$ for both the SP-INCS and the SM-INCS, and $\gamma_{(1)} = 3$ and $\delta = 0.85$ for the SP-INCS. Fig. 4(a) and (b) plots $\text{err}^d_{(k)}$ and $\text{err}^r_{(k)}$ computed by the SP-INCS and the SM-INCS, respectively. As expected, $\text{err}^d_{(k)}$ computed by the SP-INCS converges faster than that computed by the SM-INCS. On the other hand, $\text{err}^r_{(k)}$ computed by the SP-INCS converges slower. This is observed because the thresholding applied at Step 3 modifies the original Newton solution by further emphasizing the sparseness, which is not accessible by the minimization problem. The solutions recovered at the SM-INCS and SP-INCS iteration $k = 35$ in are shown in Fig. 5(a) and (b), respectively. Fig. 5(a) shows that the inner circle and the outer ring are not separated and detected as one object by the SM-INCS. On the other hand, in the solution recovered by the SP-INCS, the inner circle and the outer ring are clearly identified. Once again, results demonstrate the benefits of the sparsity constraint regularization.

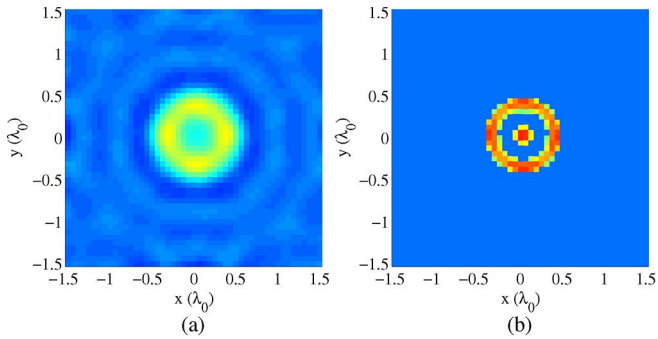

Fig. 5. Profiles recovered by the (a) SM-INCS ($\text{err}^d_{(35)} = 75.5\%$) and the (b) SP-INCS ($\text{err}^d_{(35)} = 44.1\%$) at $k = 35$.

IV. Conclusion

An INCS algorithm regularized with truncated and thresholded LW iterations is proposed for the microwave imagining of domains with sparse content. The accuracy and efficiency of the proposed scheme are increased using three methods. First, the LW iterations are preconditioned by leveling the singular values of the FD matrix. Second, an additional hard thresholding is applied at the end of each INCS iteration to remove the small ripples produced by the IN step. Finally, the weight of the L_0/L_1-norm penalty term is reduced during the INCS iterations consistently with the quadratic convergence of the iterations.

Numerical results, which demonstrate the accuracy and efficiency of the proposed method in recovering sparse and discontinuous dielectric profiles with high contrast values, are presented.

References

[1] D. Colton and R. Kress, *Inverse Acoustic and Electromagnetic Inverse Acoustic and Electromagnetic Scattering Theory*. New York, NY, USA: Springer-Verlag, 2012.

[2] S. D. Rajan and G. V. Frisk, "A comparison between the Born and Rytov approximations for the inverse backscattering," *Geophysics*, vol. 54, no. 7, pp. 864–871, Jul. 1989.

[3] Y. Wang and W. Chew, "An iterative solution of the two-dimensional electromagnetic inverse scattering problem," *Int. J. Imaging Syst. Technol.*, vol. 1, no. 1, pp. 100–108, Summer 1989.

[4] W. Chew and Y. Wang, "Reconstruction of two-dimensional permittivity distribution using the distorted Born iterative method," *IEEE Trans. Med. Imag.*, vol. 9, no. 2, pp. 218–225, Jun. 1990.

[5] A. Franchois and C. Pichot, "Microwave imaging-complex permittivity reconstruction with a Levenberg–Marquardt method," *IEEE Trans. Antennas Propag.*, vol. 45, no. 2, pp. 203–215, Feb. 1997.

[6] G. Bozza and M. Pastorino, "An inexact Newton-based approach to microwave imaging within the contrast source formulation," *IEEE Trans. Antennas Propag.*, vol. 57, no. 4, pp. 1122–1132, Apr. 2009.

[7] I. Daubechies, M. Defrise, and C. De Mol, "An iterative thresholding algorithm for linear inverse problems with a sparsity constraint," *Commun. Pure Appl. Math.*, vol. 57, no. 11, pp. 1413–1457, Nov. 2004.

[8] J. M. Bioucas-Dias and M. A. Figueiredo, "A new TwIST: Two-step iterative shrinkage/thresholding algorithms for image restoration," *IEEE Trans. Image Process.*, vol. 16, no. 12, pp. 2992–3004, Dec. 2007.

[9] A. Desmal and H. Bacý, "Shrinkage-thresholding enhanced Born iterative method for solving 2D inverse electromagnetic scattering problem," *IEEE Trans. Antennas Propag.*, vol. 62, no. 7, pp. 3878–3884, Jul. 2014.

[10] P.M. Van Den Berg and R.E. Kleinman, "A contrast source inversion method," *Inverse Probl.*, vol. 13, no. 6, pp. 1607–1620, Dec. 1997.

[11] R. C. Aster, B. Borchers, and C. H. Thurber, *Parameter Estimation and Inverse Problems*. San Diego, CA, USA: Academic, 2013.

[12] K. Belkebir and M. Saillard, "Special section: Testing inversion algorithms against experimental data," *Inverse Probl.*, vol. 17, no. 6, pp. 1565–1571, Dec. 2001.